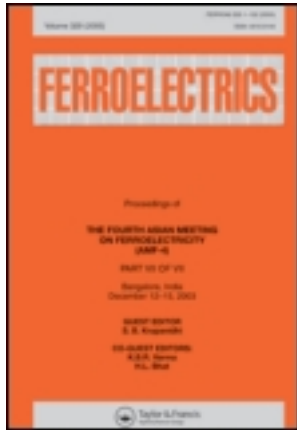


This article was downloaded by: [Pennsylvania State University]

On: 01 April 2013, At: 13:33

Publisher: Taylor & Francis

Informa Ltd Registered in England and Wales Registered Number: 1072954 Registered office: Mortimer House, 37-41 Mortimer Street, London W1T 3JH, UK



Ferroelectrics

Publication details, including instructions for authors and subscription information:

<http://www.tandfonline.com/loi/gfer20>

Impact of Free Charges on Polarization and Pyroelectricity in Antiferrodistortive Structures and Surfaces Induced by a Flexoelectric Effect

A. N. Morozovska^a, E. A. Eliseev^b, M. D. Glinchuk^b, Long Qing Chen^c, S. V. Kalinin^d & V. Gopalan^c

^a Institute of Physics, National Academy of Science of Ukraine, 03028, Kyiv, Ukraine

^b Institute for Problems of Materials Science, National Academy of Science of Ukraine, 03142, Kyiv, Ukraine

^c Department of Materials Science and Engineering, Pennsylvania State University, University Park, Pennsylvania, 16802, USA

^d Center for Nanophase Materials Science, Oak Ridge National Laboratory, Oak Ridge, TN, 37831

Version of record first published: 18 Dec 2012.

To cite this article: A. N. Morozovska, E. A. Eliseev, M. D. Glinchuk, Long Qing Chen, S. V. Kalinin & V. Gopalan (2012): Impact of Free Charges on Polarization and Pyroelectricity in Antiferrodistortive Structures and Surfaces Induced by a Flexoelectric Effect, *Ferroelectrics*, 438:1, 32-44

To link to this article: <http://dx.doi.org/10.1080/00150193.2012.744257>

PLEASE SCROLL DOWN FOR ARTICLE

Full terms and conditions of use: <http://www.tandfonline.com/page/terms-and-conditions>

This article may be used for research, teaching, and private study purposes. Any substantial or systematic reproduction, redistribution, reselling, loan, sub-licensing, systematic supply, or distribution in any form to anyone is expressly forbidden.

The publisher does not give any warranty express or implied or make any representation that the contents will be complete or accurate or up to date. The accuracy of any instructions, formulae, and drug doses should be independently verified with primary sources. The publisher shall not be liable for any loss, actions, claims, proceedings, demand, or costs or damages whatsoever or howsoever caused arising directly or indirectly in connection with or arising out of the use of this material.

Impact of Free Charges on Polarization and Pyroelectricity in Antiferrodistortive Structures and Surfaces Induced by a Flexoelectric Effect

A. N. MOROZOVSKA,^{1,*} E. A. ELISEEV,² M. D. GLINCHUK,²
LONG QING CHEN,³ S. V. KALININ,⁴ AND V. GOPALAN^{3,**}

¹Institute of Physics, National Academy of Science of Ukraine, 03028, Kyiv, Ukraine

²Institute for Problems of Materials Science, National Academy of Science of Ukraine, 03142 Kyiv, Ukraine

³Department of Materials Science and Engineering, Pennsylvania State University, University Park, Pennsylvania 16802, USA

⁴Center for Nanophase Materials Science, Oak Ridge National Laboratory, Oak Ridge, TN 37831

Landau-Ginzburg-Devonshire theory has been used to show that the combined effect of flexoelectricity and rotostriction can lead to a spontaneous polarization and pyroelectricity in the vicinity of antiphase boundaries, structural twin walls, surfaces, and interfaces in the octahedrally tilted phase of otherwise non-ferroelectric SrTiO₃. In particular, the spontaneous polarization reaches the values $\sim 0.1\text{--}5\mu\text{C}/\text{cm}^2$ at the SrTiO₃ antiphase boundaries and twins without free charges. In the current study we consider the contribution of free charges and show that the spontaneous polarization reaches the values $\sim 1\text{--}5\mu\text{C}/\text{cm}^2$ in the case. Pyroelectric coefficients also strongly increase allowing for the free charges.

Keywords Flexoelectric effect; antiferrodistortive phase; antiphase and twin boundaries

I. Introduction

Multiferroic domain walls and interfaces typically possess gradients of order parameters, such as strain, octahedral rotations, polarization, and magnetization, which can couple to induce new phenomena not present in a single-domain region of bulk material [1]. The influence of strain [2] and strain gradients [3–5] in inducing ferroelectric polarization is well known. Recently, improper ferroelectricity induced by coupling to octahedral rotations has been predicted in YMnO₃ [6], Ca₃Mn₂O₇ [7], CaTiO₃ [8, 9], and their multilayers [10].

Domain walls in perovskite oxides can possess both gradients in strain and in oxygen octahedral rotations. Note that all materials are flexoelectrics [11], and all perovskite oxides with static rotations (such as octahedral rotations which is also the case of the antiferrodistortive order parameter possess rotostriction and rotosymmetry [12].

Received August 21, 2012; in final form October 15, 2012.

Corresponding author. Email: *morozo@i.com.ua, **vxg8@psu.edu

The flexoelectric coupling, which is strong enough in many perovskites [13–17], should lead to the spontaneous polarization appearance across the structural domains walls of otherwise non-ferroelectric perovskites. Direct gradient coupling between the order parameters could lead to the oscillatory solutions and non-uniform pattern formation [18, 19].

It has been previously predicted that a spontaneous polarization can appear inside structural walls due to biquadratic coupling term [20], but it is absent in the bulk. The biquadratic coupling term can be the reason of magnetization appearance inside the ferromagnetic domain wall in non-ferromagnetic media [21]. Biquadratic coupling leads to a polarization appearance inside antiphase boundaries in SrTiO₃ below 50 K [22]. However, Zubko *et al.* [23] experimentally observed strong changes of the apparent flexoelectric coefficient in SrTiO₃ at much higher temperatures, namely below the antiferrodistortive structural phase transition temperature (105 K), and supposed its reason in the polarization appearance at the domain walls between twins. Recent experimental studies of domain wall damping and elastic softening of twin walls in SrTiO₃ reveals their polar properties and evidences that ferroelastic domain walls in SrTiO₃ become ferroelectric at low temperatures [24].

The joint action of flexoelectric effect and rotostriction (previously named roto-flexo-effect) can lead to spontaneous polarization at an interface, across which the octahedral rotations change [25–27]. In particular, it was predicted that the roto-flexo field gives rise to improper ferroelectricity and pyroelectricity in the vicinity of antiferrodistortive boundaries and elastic twins in bulk SrTiO₃ [25], as well as in the vicinity of semi-infinite SrTiO₃ surface below 105 K [26] and its thin films [27]. In the work we theoretically study the influence of the contribution of free charges on the improper polarization and pyroelectric response induced by flexo-roto effects in the SrTiO₃ structural hard and easy twin boundaries (TB) and antiphase boundaries (APB).

II. Problem Statement and Basic Equations

Following Tagantsev *et al.* [22], the free energy density has the form [25]:

$$\begin{aligned}
 F_b = & a_i(T) P_i^2 + a_{ij}^u P_i^2 P_j^2 + \dots + \frac{g_{ijkl}}{2} \left(\frac{\partial P_i}{\partial x_j} \frac{\partial P_k}{\partial x_l} \right) \\
 & - P_i \left(\frac{E_i^d}{2} + E_i^{ext} \right) - q_{ijkl} u_{ij} P_k P_l + \frac{c_{ijkl}}{2} u_{ij} u_{kl} \\
 & + b_i(T) \Phi_i^2 + b_{ij}^u \Phi_i^2 \Phi_j^2 - \eta_{ijkl}^u P_i P_j \Phi_k \Phi_l + \frac{v_{ijkl}}{2} \left(\frac{\partial \Phi_i}{\partial x_j} \frac{\partial \Phi_k}{\partial x_l} \right) \\
 & - r_{ijkl}^{(\Phi)} u_{ij} \Phi_k \Phi_l + \frac{f_{ijkl}}{2} \left(\frac{\partial P_k}{\partial x_l} u_{ij} - P_k \frac{\partial u_{ij}}{\partial x_l} \right) - \Phi_i \tau_i^d
 \end{aligned} \quad (1)$$

P_i is polarization vector, Φ_i is the components of an axial tilt vector corresponding to the octahedral rotation angles ($i = 1, 2, 3$) [12], τ_i^d is de-elasticification torque [12]; $u_{ij}(\mathbf{x})$ is the strain tensor. The summation is performed over all repeated indices.

Coefficients $a_i(T)$ and $b_i(T)$ depend on temperature in accordance with Barrett law for quantum paraelectrics [28, 29]: $a_1(T) = \alpha_T T_q^{(E)} (\coth(T_q^{(E)}/T) - \coth(T_q^{(E)}/T_0^{(E)}))$ and $b_1(T) = \beta_T T_q^{(\Phi)} (\coth(T_q^{(\Phi)}/T) - \coth(T_q^{(\Phi)}/T_S))$. Gradients coefficients are g_{ijkl} and v_{ijkl} ; f_{ijkl} is the forth-rank tensor of flexoelectric coupling, q_{ijkl} is the forth-rank electrostriction tensor, $r_{ijkl}^{(\Phi)}$ is the rotostriction tensor. The biquadratic coupling term, $\eta_{ijkl} P_i P_j \Phi_k \Phi_l$,

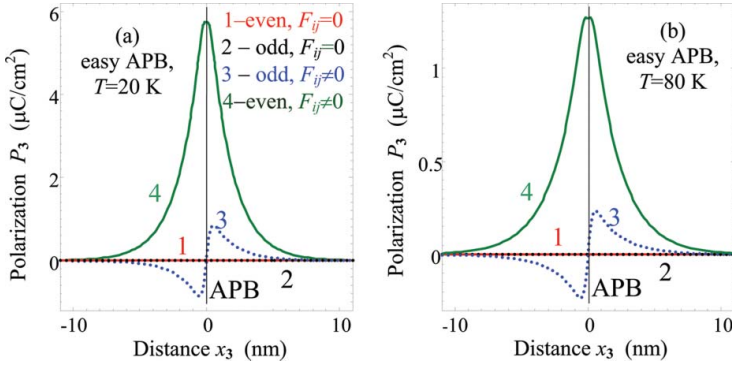


Figure 1. Spontaneous polarization distribution across easy APB calculated at temperatures $T = 20\text{ K}$ (a) and 80 K (b) for SrTiO_3 parameters; concentration of free carriers $n_0 = 10^{26}\text{ m}^{-3}$. Perpendicular to APB component P_3 -odd (dotted curves) and P_3 -even (solid curves) are calculated for nonzero flexoelectric effect $F_{ij} \neq 0$ and biquadratic coupling $\eta_{ij} \neq 0$ (curves 3, 4) and for the case of nonzero biquadratic coupling $\eta_{ij} \neq 0$ and zero flexoelectric effect $F_{ij} \equiv 0$ (curves 1, 2).

between Φ_i and polarization vector components P_i are defined by the constants η_{ijkl} [22, 30]; $r_{ijkl}^{(\Phi)}$ is rotostriction tensor, f_{ijkl} is the flexoelectric effect tensor.

Coupled Euler-Lagrange equations of state are obtained from the minimization of the free energy (1) as [25]:

$$\frac{\partial F_b}{\partial \Phi_i} - \frac{\partial}{\partial x_j} \left(\frac{\partial F_b}{\partial (\partial \Phi_i / \partial x_j)} \right) = 0 \quad (2a)$$

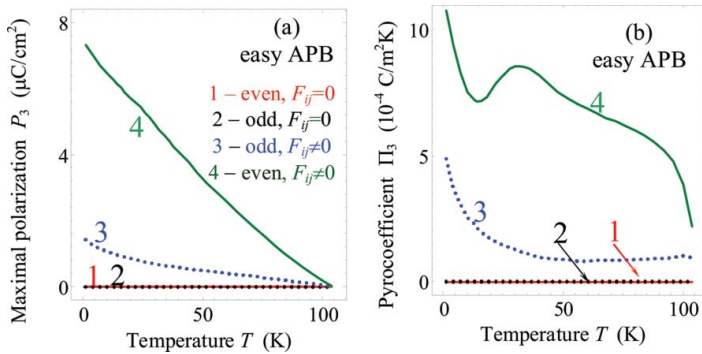


Figure 2. Temperature dependences of the spontaneous polarization maximal value (a) and (b) corresponding pyroelectric coefficient Π_3 calculated at easy APB in SrTiO_3 with concentration of free carriers $n_0 = 10^{26}\text{ m}^{-3}$. Temperature dependences are calculated for nonzero flexoelectric effect $F_{ij} \neq 0$ and biquadratic coupling $\eta_{ij} \neq 0$ (curves 3, 4) and for the case of nonzero biquadratic coupling $\eta_{ij} \neq 0$ and zero flexoelectric effect $F_{ij} \equiv 0$ (curves 1, 2). Curves 1–4 style and color coding for plots (a, b) are the same and described in the legend to plot (a). Solid and dotted curves correspond to P_3 -even and P_3 -odd solutions respectively.

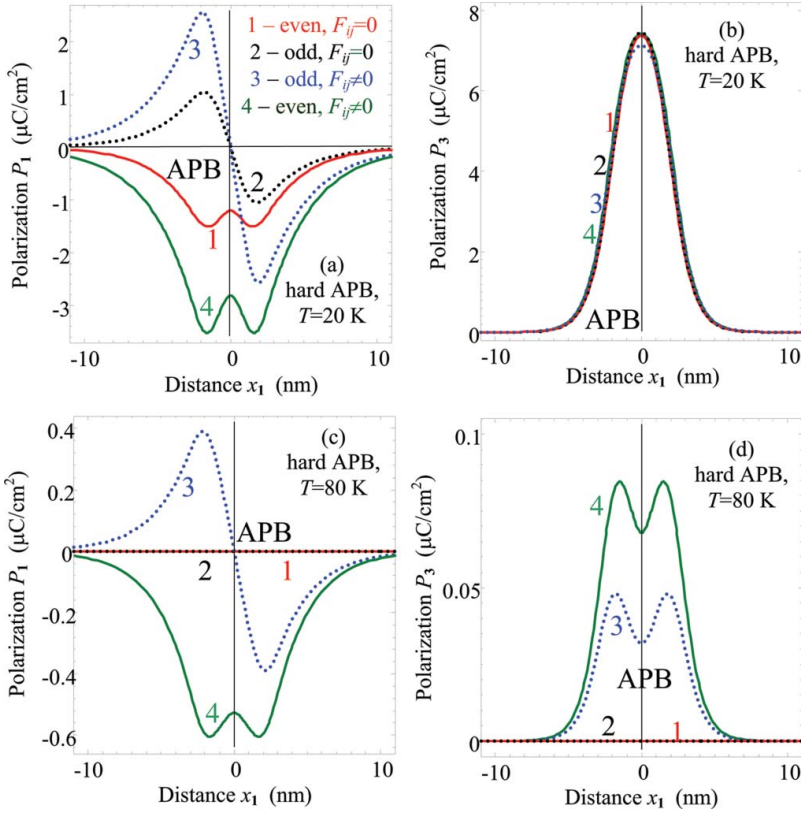


Figure 3. Spontaneous polarization distribution across hard APB calculated at temperatures $T = 20\text{ K}$ (a, b) and 80 K (c, d) for SrTiO₃ parameters, concentration of free carriers $n_0 = 10^{26}\text{ m}^{-3}$. Polarization components perpendicular (P_1) and parallel (P_3) to APB are shown. P_1 -odd (dotted curves) and P_1 -even (solid curves) are calculated for nonzero flexoelectric effect $F_{ij} \neq 0$ and biquadratic coupling $\eta_{ij} \neq 0$ (curves 3, 4) and for the case of nonzero biquadratic coupling $\eta_{ij} \neq 0$ and zero flexoelectric effect $F_{ij} \equiv 0$ (curves 1, 2). Curves 1–4 style and color coding for plots (a-d) are the same and described in the legend to plot (a).

$$\frac{\partial F_b}{\partial P_i} - \frac{\partial}{\partial x_j} \left(\frac{\partial F_b}{\partial (\partial P_i / \partial x_j)} \right) = 0 \quad (2b)$$

$$\frac{\partial F_b}{\partial u_{ij}} - \frac{\partial}{\partial x_k} \left(\frac{\partial F_b}{\partial (\partial u_{ij} / \partial x_k)} \right) = \sigma_{ij} \quad (2c)$$

where $\sigma_{ij}(\mathbf{x})$ is the stress tensor that satisfies mechanical equilibrium equation $\partial \sigma_{ij} t(\mathbf{x}) / \partial x_j = 0$. Stable solutions of the Euler-Lagrange Eq. (2) were obtained numerically by iteration method. We set initial distributions of the tilt and polarization vectors, which satisfy the boundary conditions. Special attention was paid to the parity of the obtained polarization distributions, namely we consider both odd and even initial polarization distributions with respect to the domain wall plane. Iterations were stopped, when the relative tolerance reached the value 10^{-5} .

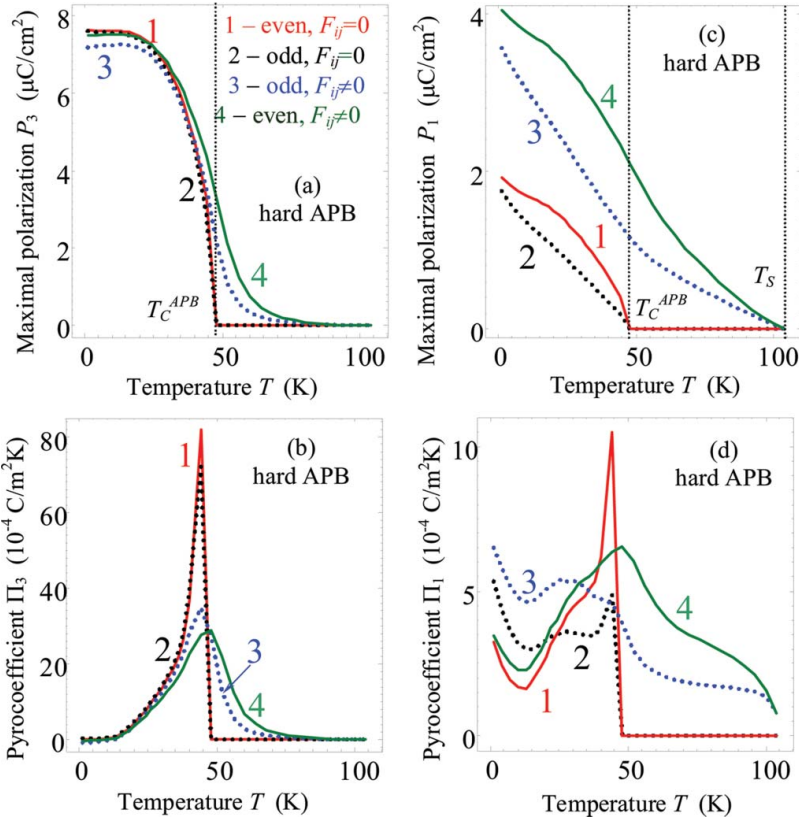


Figure 4. Temperature dependences of maximal values of spontaneous polarization components P_3 and P_1 (a, b) and corresponding pyroelectric coefficient components Π_3 and Π_1 (c, d) calculated at hard APB for SrTiO₃, concentration of free carriers $n_0 = 10^{26} \text{ m}^{-3}$. Temperature dependences are calculated for nonzero flexoelectric effect $F_{ij} \neq 0$ and biquadratic coupling $\eta_{ij} \neq 0$ (curves 3, 4) and for the case of nonzero biquadratic coupling $\eta_{ij} \neq 0$ and zero flexoelectric effect $F_{ij} \equiv 0$ (curves 1, 2). Curves 1–4 style and color coding for plots (a, b) are the same and described in the legend to plot (a). Solid and dotted curves correspond to P_3 -even and P_3 -odd solutions, respectively.

In the previous studies [25–27] we considered SrTiO₃ without free carriers and so depolarization effects were maximal. However, one can govern the free carriers concentration in SrTiO₃, as well as in other tilted perovskites, e.g. by varying concentration of the oxygen vacancies. For instance, experimental data [31, 32] report about weakly temperature dependent concentration of free carriers in SrTiO₃ that vary in the range $n_0 = (10^{22} - 5 \cdot 10^{26}) \text{ m}^{-3}$ depending on the amount of oxygen vacancies. So the question about the influence of free carriers on the spontaneous polarization and pyroelectric response of the antiphase boundaries should be studied in details. In the section we perform numerical simulations of interfacial polarization and pyroelectric response for “relatively good” semiconductor SrTiO₃ with $n_0 = (10^{24} - 10^{26}) \text{ m}^{-3}$ (but still not approaching the border of highly conductive media with $n_0 > 10^{28} \text{ m}^{-3}$) and compare obtained dependences with ones calculated in the previous section for dielectric SrTiO₃.

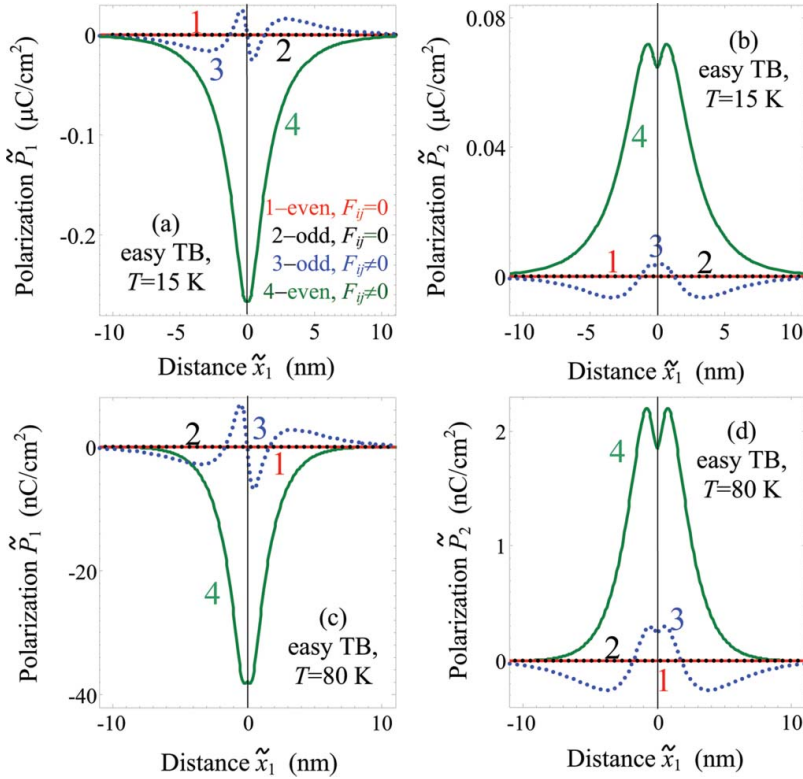


Figure 5. Spontaneous polarization distribution across easy TB calculated at temperatures $T = 15\text{ K}$ (a, b) and 80 K (c, d) for SrTiO₃ parameters, concentration of free carriers $n_0 = 10^{26}\text{ m}^{-3}$. Polarization components perpendicular (\tilde{P}_1) and parallel (\tilde{P}_2) to TB are shown. \tilde{P}_1 -odd (dotted curves) and \tilde{P}_1 -even (solid curves) are calculated for nonzero flexoelectric effect $F_{ij} \neq 0$ and biquadratic coupling $\eta_{ij} \neq 0$ (curves 3, 4) and for the case of nonzero biquadratic coupling $\eta_{ij} \neq 0$ and zero flexoelectric effect $F_{ij} \equiv 0$ (curves 1, 2). Curves 1–4 style and color coding for plots (a–d) are the same and described in the legend to plot (a).

For semiconductor SrTiO₃ the depolarization field $E_i^d = -\partial\varphi/\partial x_i$ inside the wall should be determined from the Poisson equation:

$$\frac{\partial^2\varphi}{\partial x_i^2} = -\frac{e}{\varepsilon_0\varepsilon^b}(N_d^+(\varphi) - n(\varphi) + p(\varphi)) + \frac{\partial P_i}{\varepsilon_0\varepsilon^b\partial x_i} \quad (3)$$

Ionized shallow donors $N_d^+(\varphi)$ (e.g. oxygen vacancies), and free electrons $n(\varphi)$ and holes $p(\varphi)$ concentrations φ -dependence were taken the same as in Ref. [33]. In Debye approximation $-\frac{e}{\varepsilon_0\varepsilon^b}(N_d^+ - n + p) \approx \frac{\varphi}{R_d^2}$, where $R_d = \sqrt{\varepsilon^b\varepsilon_0k_B T/(2e^2n_0)}$ is the “net” Debye screening radius, reflecting the screening by free carriers accumulated around the domain walls, n_0 is the equilibrium average concentration of the free carriers, $k_B = 1.3807 \times 10^{-23}\text{ J/K}$, where T is the absolute temperature. We checked the applicability of Debye approximation during the numerical simulations of Eq. (3) and appeared that $|\varphi| < k_B T$ up to 10 K , making Debye approximation self-consistent in the wide temperature range.

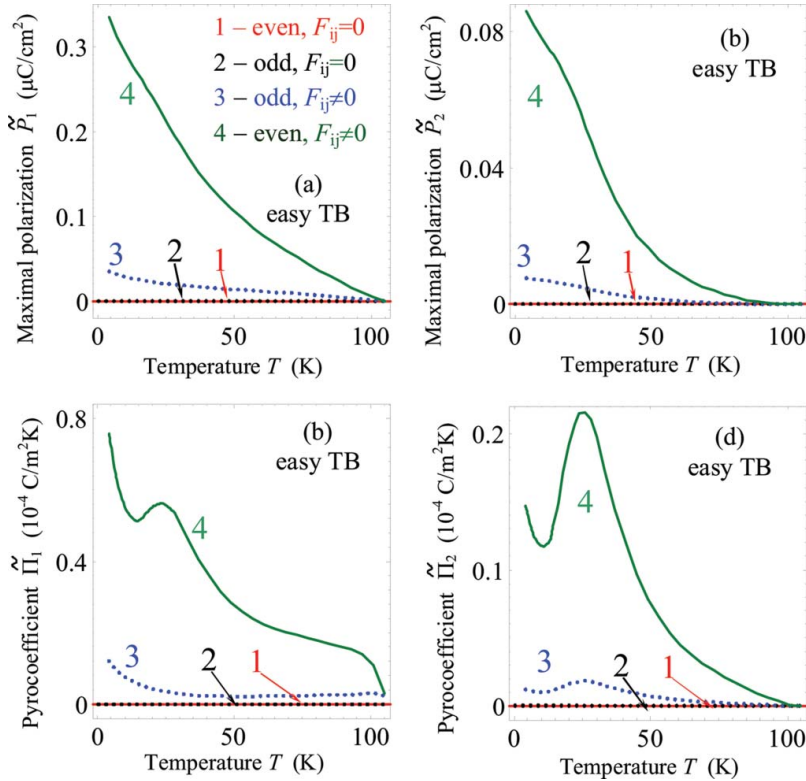


Figure 6. Temperature dependences of spontaneous polarization components \tilde{P}_1 and \tilde{P}_2 maximal values (a, b) and corresponding pyroelectric coefficient components $\tilde{\Pi}_1$ and $\tilde{\Pi}_2$ (c, d) calculated at easy TB for SrTiO₃ parameters, concentration of free carriers $n_0 = 10^{26} \text{ m}^{-3}$. Temperature dependences are calculated for nonzero flexoelectric effect $F_{ij} \neq 0$ and biquadratic coupling $\eta_{ij} \neq 0$ (curves 3, 4) and for the case of nonzero biquadratic coupling $\eta_{ij} \neq 0$ and zero flexoelectric effect $F_{ij} \equiv 0$ (curves 1, 2). Curves 1–4 style and color coding for plots (a, b) are the same and described in the legend to plot (a). Solid and dotted curves correspond to \tilde{P}_1 -even and \tilde{P}_1 -odd solutions, respectively.

III. Free Carriers Impact on the Interfacial Polarization and Pyroelectric Response

Spontaneous polarization distributions across easy and hard APB are shown in Figs. 1 and 3, correspondingly. Temperature dependences of the spontaneous polarization maximal value and pyroelectric response coefficients are shown in Figs. 2 and 4, correspondingly. Spontaneous polarization components distributions across easy and hard TB are shown in Figs. 5 and 7, correspondingly. Temperature dependences of the polarization maximal values and pyroelectric coefficients are shown in Figs. 6 and 8, correspondingly.

Interfacial polarization spatial distribution and its temperature behavior calculated for semiconductor SrTiO₃ with $n_0 = (10^{24} - 10^{26}) \text{ m}^{-3}$ appeared semi-qualitatively similar to the ones calculated for dielectric SrTiO₃ [25]. Naturally, free electrons and mobile oxygen vacancies effectively screen the depolarization field across polar interfaces and strongly enhance the components of interfacial polarization conjugated with depolarization field. Thus, several other important differences exist:

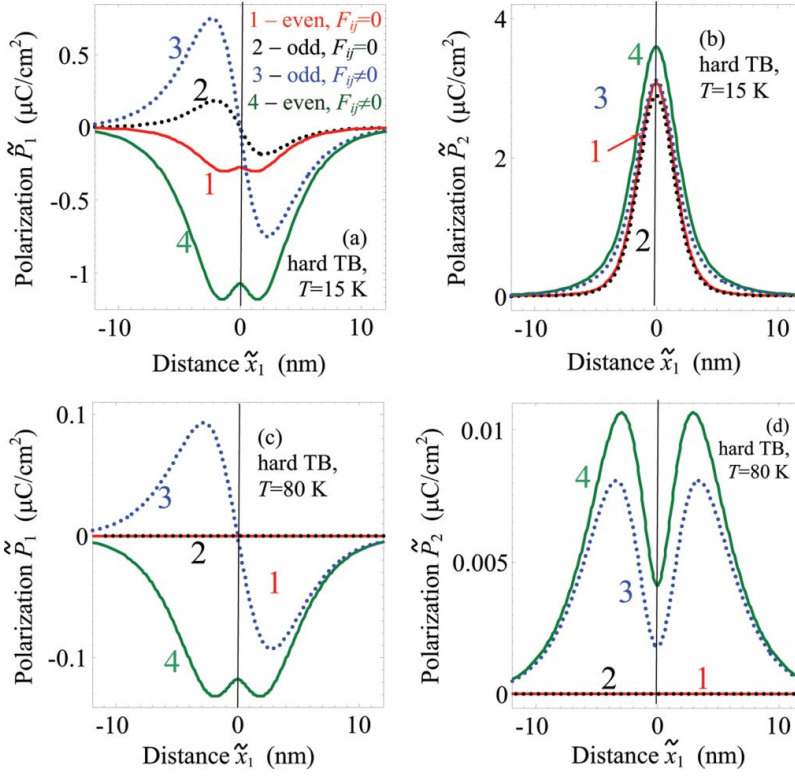


Figure 7. Spontaneous polarization distribution across hard TB calculated at temperatures $T = 15$ K (a, b) and 80 K (c, d) for SrTiO₃ parameters, concentration of free carriers $n_0 = 10^{26} \text{ m}^{-3}$. Polarization components perpendicular (\tilde{P}_1) and parallel (\tilde{P}_2) to TB are shown. \tilde{P}_1 -odd (dotted curves) and \tilde{P}_1 -even (solid curves) are calculated for nonzero flexoelectric effect $F_{ij} \neq 0$ and biquadratic coupling $\eta_{ij} \neq 0$ (curves 3, 4) and for the case of nonzero biquadratic coupling $\eta_{ij} \neq 0$ and zero flexoelectric effect $F_{ij} \equiv 0$ (curves 1, 2). Curves 1–4 style and color coding for plots (a–d) are the same and described in the legend to plot (a).

- 1) Numerical values of polarization and pyroelectric response across easy APB and easy TB appeared much higher (up to 100 times for $n_0 = 10^{26} \text{ m}^{-3}$!) for semiconductor SrTiO₃ than for the dielectric one (compare Figs. 1–8 with results presented in Ref. [25]). The polarization component, that is perpendicular to the wall plane, increases with the carrier concentration increase due to much smaller depolarization field, which decrease comes from the screening carriers.
- 2) The values of polarization component parallel to the hard APB or hard TB plane also increase (up to 10 times at higher temperatures) with the carrier concentration increase. Since the component is not directly affected by the depolarization field, the increase originated from the coupling with parallel component (compare Figs. 3 and 7 with figures from Ref. [25], correspondingly).
- 3) The wall width of easy APB and TB (as well as the width of the polarization component perpendicular to the hard APB or TB plane) significantly increases in the semiconductor SrTiO₃, up to 5 times for the polarization component perpendicular to the wall plane (compare x -axes scale in Figs. 1, 3, 5, 7 with the ones in Ref. [25]).

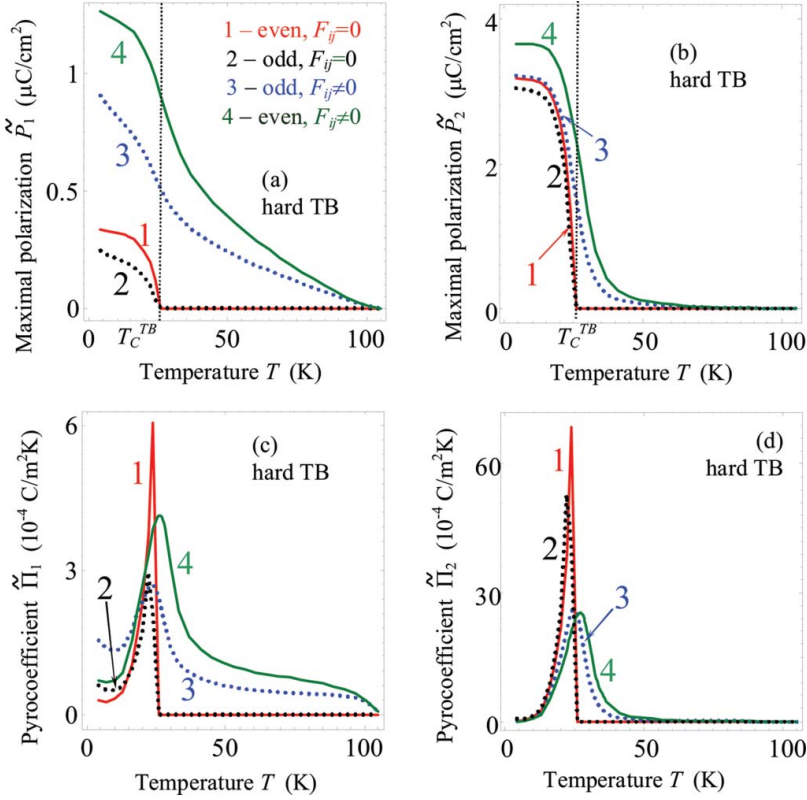


Figure 8. Temperature dependences of spontaneous polarization components \tilde{P}_1 and \tilde{P}_2 maximal values (a, b) and corresponding pyroelectric coefficient components $\tilde{\Pi}_1$ and $\tilde{\Pi}_2$ (c, d) calculated at hard TB for SrTiO₃ parameters, concentration of free carriers $n_0 = 10^{26} \text{ m}^{-3}$. Temperature dependences are calculated for nonzero flexoelectric effect $F_{ij} \neq 0$ and biquadratic coupling $\eta_{ij} \neq 0$ (curves 3, 4) and for the case of nonzero biquadratic coupling $\eta_{ij} \neq 0$ and zero flexoelectric effect $F_{ij} \equiv 0$ (curves 1, 2). Curves 1–4 style and color coding for plots (a, b) are the same and described in the legend to plot (a). Solid and dotted curves correspond to \tilde{P}_1 -even and \tilde{P}_1 -odd solutions, respectively.

The reason for the width increase with free carriers concentration increase is the depolarization field decrease. The parallel component depends on the perpendicular one via the biquadratic coupling terms, therefore the wall width of the polarization component parallel to the hard APB and hard TB also increases with the carriers concentration increase, but the effect is weaker.

- 4) Temperature dependence of the maximal polarization at easy APB or TB (as well as the polarization component perpendicular to the hard APB or TB plane) has no saturation at low temperatures in semiconductor SrTiO₃, in contrast to the dielectric SrTiO₃ (see e.g. Figs. 2, 4, 6, 8 and compare with Ref. [25]). Moreover, maximal polarization of easy antiphase boundaries super-linearly increases with the temperature decrease. The increase originated from the decrease of the depolarization field with the temperature increase. Really, in accordance with Debye equation $\frac{\partial^2 \varphi}{\partial x_i^2} \approx \frac{\varphi}{R_d^2} + \frac{\partial P_i}{\varepsilon_0 \varepsilon^b \partial x_i}$ for depolarization field $E_i^d = -\partial \varphi / \partial x_i$, the

- field decreases with the temperature increase, since the Debye screening radius $R_d = \sqrt{\varepsilon^b \varepsilon_0 k_B T / (2e^2 n_0)}$ decreases.
- 5) Pyroelectric coefficients increase with free carrier concentration increase and demonstrate additional peculiarities (maxima and minima) at temperatures below the effective Curie temperatures. Pyroelectric coefficients of easy antiphase boundaries super-linearly increase with the temperature decrease, since the polarization increases with the temperature decrease via the decrease of the Debye screening radius.

It is seen from Fig. 9a that APB energy is rather weakly dependent on the polarization distribution and its screening conditions. It is seen from Fig. 9b that TB energy looks almost independent on these factors, since the polarization component perpendicular to the TB plane is very small. The explanation is the weak dependence of the wall energy on the electric contribution. Relative electric energies of the APBs counted from the lowest P_3 -odd

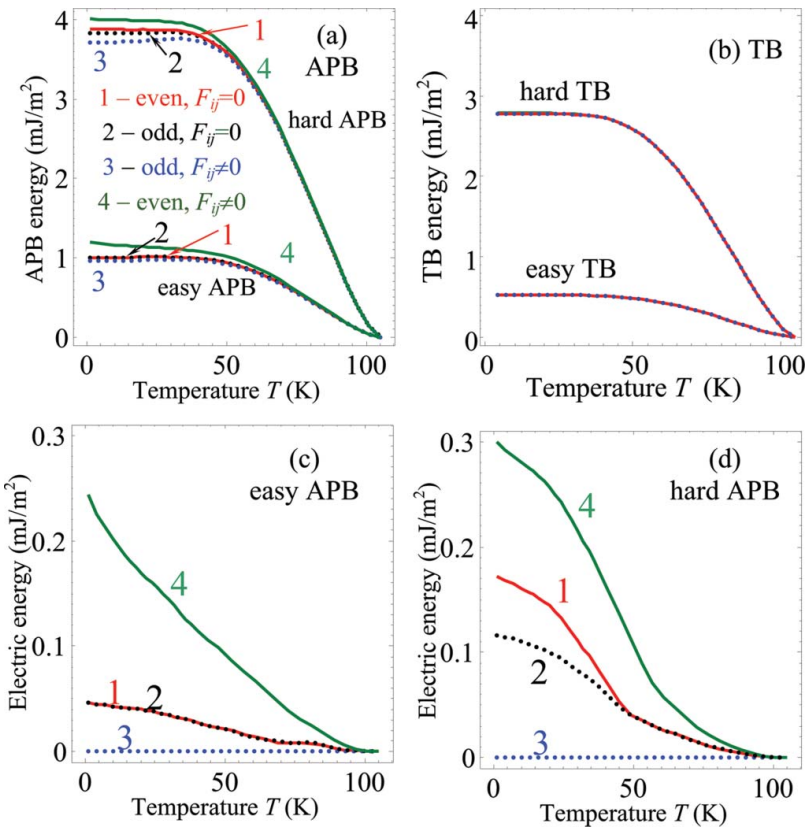


Figure 9. Energies of (a) antiphase and (b) twin boundaries vs. temperature calculated for SrTiO₃ with concentration of free carriers $n_0 = 10^{26} \text{ m}^{-3}$. Relative electric energies of easy (c) and hard (d) APBs counted from the lowest P_3 -odd solution (curves 3 on plots (a) and (b)). Temperature dependences are calculated for nonzero flexoelectric effect $F_{ij} \neq 0$ and biquadratic coupling $\eta_{ij} \neq 0$ (curves 3, 4) and for the case of nonzero biquadratic coupling $\eta_{ij} \neq 0$ and zero flexoelectric effect $F_{ij} \equiv 0$ (curves 1, 2). Solid and dotted curves correspond to P_3 -even and P_3 -odd solutions respectively. Curves 1–4 style and color coding for plots (a–d) are the same and described in the legend to plot (a).

Table 1
Influence of the free carriers concentration n_0 .

Polarization and pyro-coefficients	Hard 180-degree tilt APB and Hard 90-degree tilt TB	Easy 180-degree tilt APB and Easy 90-degree tilt TB
Parallel components P_{\parallel} and Π_{\parallel}	Increase with n_0 increase	Identically zero for easy APB Appear for easy TB and increases with n_0 increase
Perpendicular components P_{\perp} and Π_{\perp}	Strongly increase with n_0 increase due to the depolarization field decrease	Strongly increase with n_0 increase due to the depolarization field decrease

solution (curves 3 on plots (a) and (b)) are shown in Figs. 9c and 9d for easy and hard APBs, correspondingly. Similarly to the case of dielectric SrTiO₃, P_3 -even polarization distributions have the highest energy, but the electric energy difference between all types of polarization solutions is very small and super-linearly decreases with temperature increase; for TB (not shown) the difference is even smaller than for APB.

IV. Conclusions

Flexoelectric and rotostriction effects, which can give rise to the appearance of improper spontaneous polarization and pyroelectricity across APB and TB in SrTiO₃ [25–27], are facilitated by the presence of free carriers (Table 1). Free electrons and mobile oxygen vacancies can effectively screen the depolarization field across polar interfaces and strongly enhance the components of interfacial polarization conjugated with depolarization field. The spontaneous polarization reaches the values $\sim 0.1\text{--}5\mu\text{C}/\text{cm}^2$ at the SrTiO₃ antidiortive and twin boundaries without free charges [25] and $\sim 1\text{--}5\mu\text{C}/\text{cm}^2$ allowing for free charges. Our theoretical results are in qualitative agreement with experimental results [23, 24].

Acknowledgments

Authors gratefully acknowledge multiple discussions with Daniel Litvin and Behera K. Rakesh. National Science Foundation (DMR-0908718, DMR-0820404, DMR-1210588) are acknowledged by V.G., L.Q.C. A.N.M., E.A.E., M.D.G. acknowledges Ukrainian State Fund for Fundamental Researches, joint project SFFR-NSF. Research was supported (for S.V.K.) by the U.S. Department of Energy, Basic Energy Sciences, Materials Sciences and Engineering Division.

References

1. E. A. Eliseev, A. N. Morozovska, M. D. Glinchuk, B. Y. Zaulychny, V. V. Skorokhod, and R. Blinc, Surface-induced piezomagnetic, piezoelectric, and linear magnetoelectric effects in nanosystems. *Phys. Rev. B* **82**, 085408 (2010).
2. D. A. Tenne, A. Bruchhausen, N. D. Lanzillotti-Kimura, A. Fainstein, R. S. Katiyar, A. Cantarero, A. Soukiassian, V. Vaithyanathan, J. H. Haeni, W. Tian, D. G. Schlom, K. J. Choi, D. M. Kim, C. B. Eom, H. P. Sun, X. Q. Pan, Y. L. Li, L.-Q. Chen, Q. X. Jia, S. M. Nakhmanson, K. M. Rabe,

- and X. X. Xi, Probing nanoscale ferroelectricity by ultraviolet raman spectroscopy. *Science* **313**, 1614–1616 (2006).
3. E. V. Bursian, and O. I. Zaikovskii, Changes in the curvature of a ferroelectric film due to polarization. *Fiz. Tverd. Tela.* **10**, 1413 (1968) [*Sov. Phys. Solid State* **10**, 1121 (1968)]; E.V. Bursian, O.I. Zaikovskiy, and K.V. Makarov, Polarization of ferroelectric film by bending and bending deformation in the electric field. *J. Phys. Soc. Jpn.* **28**, Suppl. 416 (1970).
 4. W. Ma, and L. E. Cross, Large flexoelectric polarization in ceramic lead magnesium niobate. *Appl. Phys. Lett.* **79**, 4420 (2001).
 5. W. Ma, and L. E. Cross, Flexoelectricity of barium titanate. *Appl. Phys. Lett.* **88**, 232902 (2006).
 6. C. J. Fennie, and K. M. Rabe, The ferroelectric transition in YMnO_3 from first principles. *Phys. Rev. B* **72**, 100103(R) (2005).
 7. N. A. Benedek, and C. J. Fennie, Improper ferroelectricity: A mechanism for controllable polarization-magnetization coupling. *Phys. Rev. Lett.* **106**, 107204 (2011).
 8. L. Goncalves-Ferreira, S. A.T. Redfern, E. Artacho, and E. K.H. Salje, Ferrielectric twin walls in CaTiO_3 . *Phys. Rev. Lett.* **101**, 097602 (2008).
 9. S. Van Aert, S. Turner, R. Delville, D. Schryvers, G. Van Tendeloo, and E. K.H. Salje, Ferrielectricity at ferroelastic domain boundaries in CaTiO_3 by electron microscopy. *Adv. Mater.* **24**, 523–527 (2012).
 10. E. Bousquet, M. Dawber, N. Stucki, C. Lichtensteiger, P. Hermet, S. Gariglio, J.-M. Triscone, and P. Ghosez, Improper ferroelectricity in perovskite oxide artificial superlattices. *Nature* **452**, 732 (2008).
 11. A. K. Tagantsev, Piezoelectricity and flexoelectricity in crystalline dielectrics. *Phys. Rev. B* **34**, 5883–5889 (1986).
 12. V. Gopalan, and D. B. Litvin, Rotation-reversal symmetries in crystals and handed structures. *Nat. Mater.* **10**, 376–381 (2011).
 13. M. S. Majdoub, P. Sharma, and T. Cagin, Enhanced size-dependent piezoelectricity and elasticity in nanostructures due to the flexoelectric effect. *Phys. Rev. B* **77**, 125424 (2008).
 14. G. Catalan, B. Noheda, J. McAnaney, L. J. Sinnamon, and J. M. Gregg, Strain gradients in epitaxial ferroelectrics. *Phys. Rev. B* **72**, 020102 (2005).
 15. E. A. Eliseev, A. N. Morozovska, M. D. Glinchuk, and R. Blinc, Spontaneous flexoelectric/flexomagnetic effect in nanoferroics. *Phys. Rev. B* **79**, 165433 (2009).
 16. D. Lee, A. Yoon, S. Y. Jang, J.-G. Yoon, J.-S. Chung, M. Kim, J. F. Scott, and T. W. Noh, Giant flexoelectric effect in ferroelectric epitaxial thin films. *Phys. Rev. Lett.* **107**, 057602 (2011).
 17. I. Ponomareva, A. K. Tagantsev, and L. Bellaiche, Finite-temperature flexoelectricity in ferroelectric thin films from first principles. *Phys. Rev. B* **85**, 104101 (2012).
 18. T. A. Aslanian, and A. P. Levanyuk, On the possibility of the incommensurate phase near $\alpha \rightleftharpoons \beta$ transition point in quartz. *Pis'ma Zh. Eksp. Teor. Fiz.* **28**, 76, (1978). [*Soviet Phys. JETP Lett.* **28**, 70, (1978).]
 19. B. Houchmanzadeh, J. Lajzerowicz, and E. Salje, Interfaces and ripple states in ferroelastic crystals - A simple model. *Phase Trans.* **38**, 77 (1992).
 20. B. Houchmanzadeh, J. Lajzerowicz, and E. Salje, Order parameter coupling and chirality of domain walls. *J. Phys.: Condens. Matter* **3**, 5163 (1991).
 21. M. Daraktchiev, G. Catalan, and J. F. Scott, Landau theory of ferroelectric domain walls in magnetoelectrics. *Ferroelectrics* **375**, 122 (2008).
 22. A. K. Tagantsev, E. Courtens, and L. Arzel, Prediction of a low-temperature ferroelectric instability in antiphase domain boundaries of strontium titanate. *Phys. Rev. B* **64**, 224107 (2001).
 23. P. Zubko, G. Catalan, A. Buckley, P. R.L. Welche, and J. F. Scott, Strain-gradient-induced polarization in SrTiO_3 single crystals. *Phys. Rev. Lett.* **99**, 167601 (2007).
 24. J. F. Scott, E. K.H. Salje, and M. A. Carpenter, Domain wall damping and elastic softening in SrTiO_3 : evidence for polar twin walls. *Phys. Rev. Lett.* (2012) (to be published).
 25. A. N. Morozovska, E. A. Eliseev, M. D. Glinchuk, L.-Q. Chen, and V. Gopalan, Interfacial polarization and pyroelectricity in antiferrodistortive structures induced by a flexoelectric effect and rotostriction. *Phys. Rev. B* **85**, 094107 (2012).

26. A. N. Morozovska, E. A. Eliseev, S. V. Kalinin, L.-Q. Chen, and V. Gopalan, Surface polar states and pyroelectricity in ferroelastics induced by flexo-rotor field. *Appl. Phys. Lett* **100**, 142902 (2012).
27. A. N. Morozovska, E. A. Eliseev, S. L. Bravina, A. Y. Borisevich, and S. V. Kalinin, Roto-flexoelectric coupling impact on the phase diagrams and pyroelectricity of thin SrTiO₃ films. *J. Appl. Phys.* **112**, 064111 (2012).
28. P. A. Fleury, and J. M. Worlock, Electric-field-induced raman scattering in SrTiO₃ and KTaO₃. *Phys. Rev.* **174**, 613 (1968).
29. P. A. Fleury, J. F. Scott, and J. M. Worlock, Soft phonon modes and the 110°K phase transition in SrTiO₃. *Phys. Rev. Lett.* **21**, 16–19 (1968).
30. M. J. Haun, E. Furman, T. R. Halemane, and L. E. Cross, Thermodynamic theory of the lead zirconate-titanate solid solution system, part IV: Tilting of the oxygen octahedra. *Ferroelectrics* **99**, 13 (1989).
31. R. Moos, W. Mcnesklou, and K. H. Hardtl, Hall mobility of undoped n-type conducting strontium titanate single crystals between 19 K and 1373 K. *Appl. Phys. A* **61**, 389 (1995).
32. R. Moos, and K. H. Hardtl, Electronic transport properties of Sr_{1-x}La_xTiO₃ ceramics. *J. Appl. Phys.* **80**, 393 (1996).
33. E. A. Eliseev, A. N. Morozovska, G. S. Svechnikov, V. Gopalan, and V. Y. Shur, Static conductivity of charged domain walls in uniaxial ferroelectric semiconductors. *Phys. Rev. B* **83**, 235313 (2011).